CHEMISTRY OF MATERIALS

Article

pubs.acs.org/cm

Nanoscale Investigation of Solid Electrolyte Interphase Inhibition on Li-Ion Battery MnO Electrodes via Atomic Layer Deposition of Al_2O_3

Albert L. Lipson,[†] Kanan Puntambekar,[†] David J. Comstock,[‡] Xiangbo Meng,[‡] Michael L. Geier,[†] Jeffrey W. Elam,[‡] and Mark C. Hersam*[,†]

[†]Department of Materials Science and Engineering, Northwestern University, Evanston, Illinois 60208, United States

[‡]Energy Systems Division, Argonne National Laboratory, Lemont, Illinois 60439, United States

ABSTRACT: Application of a functional surface coating on Li-ion battery electrodes can potentially result in a significant enhancement of the lifespan of the battery cell. In particular, atomic layer deposition (ALD), which can create highly conformal ultrathin oxide films on many different electrodes has been shown to increase the cyclability in these systems. In this study, we explore the impact of such films on the formation of the solid electrolyte interphase (SEI), which may explain why these films show improvements in the cycling performance. Specifically, we characterize, using in situ scanning ion conductance microscopy and other ex situ surface characterization techniques, the SEI formed on ALD Al_2O_3 coated and uncoated MnO electrodes. We ascertain that ~9 Å is the minimum thickness of ALD Al_2O_3 that will inhibit thick SEI formation. Furthermore, we show that the ALD surface coating is robust and prevents SEI formation for at least 100 cycles. Lastly, we investigated the differences between our in situ and ex situ measurements to help determine what artifacts can result that are due to post-processing for ex situ studies.

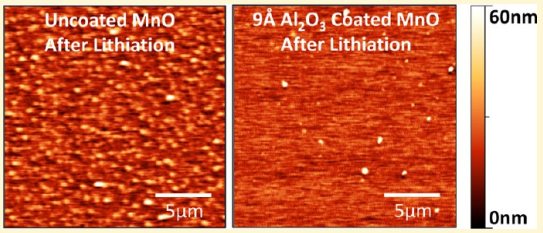

INTRODUCTION

As next-generation applications for Li-ion batteries emerge in the transportation sector, the benefits of higher electrode capacity need to be balanced against stringent requirements for safety and reliability. In this regard, the solid electrolyte interphase (SEI) plays a critical role and thus methods for controlling the SEI hold promise for achieving optimal performance. The SEI forms via the decomposition of the electrolyte on battery electrode surfaces.[1,2] Depending on the components of the electrolyte, a variety of compounds can form in the SEI layer including LiF, Li_2O, Li_2CO_3, R-OCO_2Li (where R is an organic group), and oligomers.[3−5] The extent and composition of the SEI is controlled by the composition of the electrodes, the battery storage conditions, and the cycling method.[6,7] The SEI can be instrumental for passivating the electrode surfaces, thereby preventing uncontrolled decomposition of the electrolyte that often leads to unsafe operating conditions.[8]

Despite the apparent advantages of the SEI, the fixed quantity of Li in a battery implies that any sequestration of Li into the SEI reduces the usable capacity. One solution to this problem is to replace the SEI with a coating that protects the electrodes without consuming Li. For instance, carbon coatings have been applied to cathode materials to improve the electrical conductivity,[9] and sol−gel deposited metal oxides have been shown to improve the longevity of battery electrodes.[10−12] Furthermore, a less reactive and more stable battery material can enhance the overall electrode performance.[13] Toward this end, atomic layer deposition (ALD) has attracted significant attention for both the fabrication of battery electrode materials and the deposition of metal oxide coatings on battery electrodes.[14]

ALD allows for highly conformal coatings with angstrom-level thickness control even on high surface area samples such as nanoparticles and aerogels.[15−17] Empirically, ultrathin conformal coatings of alumina (Al_2O_3) deposited by ALD onto battery cathodes and anodes, such as $LiCoO_2$, graphite, and Si, have shown improvements in the cycling performance.[16,18−27] For example, an approximately 5 Å Al_2O_3 coating on a lithium cobalt oxide ($LiCoO_2$) cathode reduced the capacity fade by 3-fold after 200 electrochemical cycles.[18] Ab initio modeling has also been performed to determine the mechanisms by which Li can pass through the Al_2O_3.[28,29] Both theoretical and experimental studies have demonstrated that these coatings have the potential to reduce the amount of SEI formed on anodes and proposed that this SEI suppression is primarily due to the ALD coating that blocks the electron transfer process.[30] These results suggest that the behavior of these coatings should be relatively independent of the choice of anode material.

While ALD-based SEI control has been shown to yield improvements in Li-ion battery performance in macroscopic device testing, nanometer-scale characterization of this phenomenon has not been performed either using ex situ or

Received: July 22, 2013
Revised: December 20, 2013
Published: January 7, 2014

in situ methods. Previously, a variety of in situ scanning probe microscopy (SPM) techniques have been shown to be effective for nanometer-scale characterization of Li-ion battery electrodes. In particular, in situ atomic force microscopy (AFM) has been extensively utilized for determining electrode topography as a function of electrochemical cycling.[31−37] Other AFM-based methods, such as scanning electrochemical microscopy (SECM), provide opportunities for further characterization of the sample lithiation process at a microscopic scale.[38−40] Recently, a method based on scanning ion conductance microscopy (SICM) has also been used to spatially map and correlate the topography and electrochemical changes in situ.[41]

Herein, we present the first direct nanoscale investigation of SEI formation on ALD Al_2O_3-coated anodes using in situ SICM and other ex situ surface characterization techniques. In particular, we determine that a coating of only 9 Å of ALD Al_2O_3 can practically eliminate SEI formation on the MnO anode. Furthermore, we demonstrate that this coating can survive and inhibit SEI formation for at least 100 electrochemical cycles. Lastly, we compare the effectiveness of in situ and ex situ surface characterization methodologies at observing SEI formation, thereby delineating the artifacts that can occur in ex situ measurements, such as electrolyte residues.

EXPERIMENTAL SECTION

An exceptionally flat and smooth surface is required for scanning probe microscopy based studies of SEI formation. To achieve a smooth anode surface for this work, a copper thin film current collector was deposited on a glass or sapphire substrate and subsequently capped with an ALD MnO thin film.[42−44] MnO is known to be an anode material that undergoes a conversion to Li_2O and Mn metal upon lithiation, with a theoretical capacity of 756 mAh/g.[45−47] Previous studies of the SEI on MnO using ex situ AFM imaging and nanoindentation showed an inhomogeneous and topographically rough SEI.[48] However, MnO does not suffer from the rapid cracking during cycling as is observed in high capacity anode materials such as silicon.[49] These attributes make MnO an ideal candidate for SPM studies that can elucidate how ALD coatings affect SEI formation.

The samples in this study were prepared on either Decontam (ESPI metals) cleaned glass slides or *c*-axis sapphire wafers (University Wafer). Approximately 25 nm of copper was sputter-deposited on these substrates using a Desk III sputtering system (Denton Vacuum). MnO was then deposited at 150 °C in a custom ALD reactor using $Mn(EtCp)_2$ at 80 °C and water at room temperature as the precursors. A 1s pulse was used for both precursors with a 5 s N_2 purge between precursors. 1200 ALD cycles were performed to deposit a 123 nm thick MnO film as determined by ellipsometry (J.A. Woollam M2000U). ALD Al_2O_3 was deposited in a Savannah ALD reactor (Cambridge Nanotech) using trimethylaluminum and water at 150 °C using 0.015 s pulses and 12 s of purge time. Using 3, 10, and 100 cycles of ALD Al_2O_3, the deposited ALD thicknesses are approximately 3 Å, 9 Å, and 90 Å, respectively, as determined by ellipsometry and AFM. The RMS surface roughness of these samples with or without ALD Al_2O_3 coating is approximately 1 nm for sapphire substrates and 2.5 nm for glass substrates. Striped samples were prepared via a lift off technique using NR9−1000PY (Futurrex) negative photoresist (process details and AFM images are included in the Supporting Information).

Electrochemical cycling was performed in 314 stainless steel coin cells using Celgard 2320 separators and lithium metal as the counter electrode. The top contact was made in the coin cell by wrapping copper foil around from the backside to the edges of the sample. The remaining exposed electrode area, the MnO thickness, and the standard density of MnO (5.37 g/cm^3)[50] were used to determine the active mass. The electrolyte was 1 M $LiPF_6$ (Novolyte) in 1:1 by volume ethylene carbonate and dimethyl carbonate (Sigma Aldrich). All coin cells were galvanostatically cycled at 150 mA/g between 0 and 2 V using an Arbin BT2143 battery charger. Background capacity of the coin cell, calculated using a bare glass substrate, was subtracted from the capacity curves with a scaling factor such that no capacity was below 0 mAh/g.

In situ SICM in an argon atmosphere glovebox (<1 ppm O_2 and H_2O) was performed using the techniques and equipment discussed previously.[41] Ex situ scanning electron microscopy (SEM) and X-ray photoelectron spectroscopy (XPS) were taken on samples that were removed from the coin cell in the glovebox and then rinsed in anhydrous isopropanol (Sigma Aldrich). The remaining isopropanol was wicked off with a Kimwipe. The rinsing and drying steps were repeated 2−3 times in an attempt to remove the residual electrolyte with minimal damage to the SEI layer. SEM (Hitachi SU8030) of the sample surface was taken using 30 kV electrons with no surface pretreatment. Focused ion beam (FIB) milled cross-sectional SEM was performed using a dual beam FIB/SEM (FEI Helios Nanolab). The sample surface was protected by a layer of sputter-deposited tungsten, followed by ion beam induced deposition of platinum during the FIB process. Cross-sectional SEM images were taken at a 52° angle to the sample surface using 20 keV electrons. SEM and EDS of the striped sample were taken with a S4800 SEM (Hitachi) at 5 kV and 30 kV accelerating voltage, respectively. Ex situ AFM was measured using a CP Research (Thermomicroscopes) AFM in contact mode and a Bruker Dimension Icon AFM in tapping mode.

RESULTS & DISCUSSION

Electrochemical cycling experiments were performed prior to a detailed surface characterization study. MnO thin film anodes were coated with varying thicknesses of ALD Al_2O_3 and electrochemically cycled, as shown in Figure 1. The bare MnO

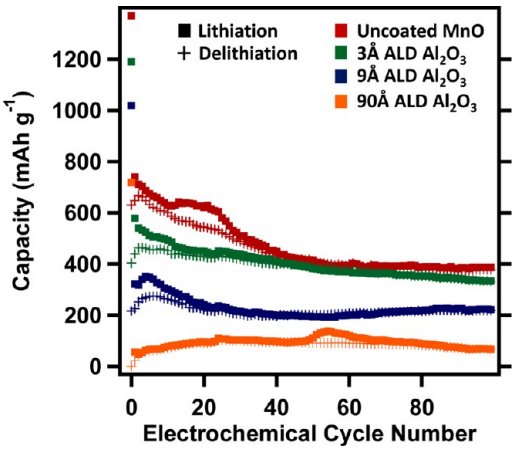

Figure 1. Electrochemical cycling performance of MnO at a rate of 150 mA/g with varying thicknesses of ALD-deposited Al_2O_3.

film shows a large capacity loss as a function of number of cycles, with the delithiation capacity dropping by about 45% from the peak to the 100th cycle. Comparatively, the ALD coated MnO films are more stable. For example, with a 3 Å Al_2O_3 coating, the delithiation capacity decreases by roughly 30% from the peak to the 100th cycle, and with a 9 Å Al_2O_3 coating the delithiation capacity decreases by only 20%. We also note that the delithiation capacity increases in these MnO films for the first few cycles, which may be occurring due to improved kinetics from the expansion of MnO or small cracks being created. This effect is larger in the coated samples, since there are likely changes to the Al_2O_3 atomic structure during initial cycling that improve Li^+ diffusion.

To determine if the decrease in the observed capacity of the ALD coated MnO as compared to the uncoated MnO was a

dx.doi.org/10.1021/cm402451h | *Chem. Mater.* 2014, 26, 935−940

kinetic or thermodynamic effect, cycling was performed at different rates. When cycled at the rate of 150 mA/g, 9 Å of ALD Al_2O_3 coating results in ~45% reduction of the capacity as shown in Figures 1 and 2. However, when the rate is reduced

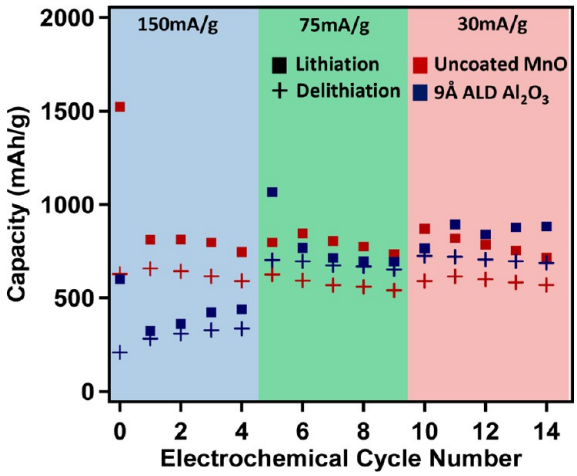

Figure 2. Comparison of electrochemical capacity at different charge and discharge rates for uncoated MnO and MnO with 9 Å of ALD Al_2O_3.

by half to 75 mA/g, the capacity of the MnO electrode with the same coating is observed to be higher than the uncoated MnO. This capacity being higher than the uncoated MnO is likely due to decreased degradation of the coated sample during the first 5 cycles, which could be caused by the reduced capacity or the coating preventing degradation. This observation indicates that the ALD Al_2O_3 film can act as a diffusion barrier for Li ions, thereby slowing the kinetics and causing some reduction in the rate capability, but not changing the actual capacity of the electrode. This effect can be mitigated by cycling at elevated temperatures,[51] or increasing the surface area.[52] We also note that there is additional irreversible capacity at slower rates for the coated sample. This effect is likely caused by the increased capacity at slower rates as well as from the coin cell materials. This electrochemical cycling study thus suggested a strong influence of the ALD surface modification on the electrode performance, which prompted a detailed nanoscale investigation of this surface during the cycling process.

In situ SICM imaging was used to gain an understanding of the surface evolution and SEI formation during the lithiation process. Topographic SICM images of MnO anodes with and without a 9 Å Al_2O_3 coating after lithiation to 0 V are shown in Figure 3. The topography of the uncoated MnO anode (Figure 3a) shows many small protrusions with an average height of ~30 nm and an increased surface roughness of 3.5 nm RMS, compared to 2.5 nm RMS before lithiation. On the other hand, the 9 Å Al_2O_3-coated MnO (Figure 3b) shows only a few tall protrusions on the surface and a relatively unchanged surface roughness of 2.5 nm RMS. These occasional protrusions on the alumina coated sample may be dust or other contaminants, or may result from enhanced SEI growth at pinholes in the thin alumina film. Nevertheless, the topographic SICM images illustrate that the ALD Al_2O_3 film effectively prevents surface roughening, which likely implies suppression of SEI growth.

Ex situ scanning electron microscopy (SEM) and X-ray photoelectron spectroscopy (XPS) measurements provide further confirmation that the ALD Al_2O_3 indeed survives electrochemical cycling and helps prevent SEI formation. Figure 4 shows SEM micrographs of the top surface and cross sections of MnO thin films, with and without an Al_2O_3 coating, after 100 electrochemical cycles. The bare MnO shows a large number of protrusions on the surface (Figure 4a), whereas the Al_2O_3 coated MnO shows only a few such protrusions, although a large network of cracks can be seen on the surface (Figure 4b). These cracks are likely a result of the alumina film and surface MnO fracturing during the expansion and contraction of the underlying MnO during cycling. The cracks may slightly increase the Li^+ diffusion into the MnO, but because of their large separation and the slow Li diffusion in MnO, the vast majority of the Li should still be entering through the Al_2O_3 coating. These cracks also appear not to have substantial SEI growth and do not appear to have destroyed the integrity of the Al_2O_3 even after 100 cycles. The cross-sectional SEM images of the samples (Figure 4c, d) further highlight the effects of the ALD coating, and in particular show a significant reduction in surface roughness. An additional thin film (indicated by the blue arrow in Figure 4c) with different contrast can be seen on the surface of the uncoated MnO that is about 60 nm thick after electrochemical cycling. Because there is no equivalent layer in the Al_2O_3-coated MnO sample, the additional film in the uncoated MnO case is likely attributable to the SEI layer. Furthermore, Al_2O_3 was detected by XPS after 100 electrochemical cycles, indicating that it at least partially survives cycling. Also, XPS indicates that the composition of the SEI formed on coated and uncoated MnO is nearly identical (see the Supporting Information for XPS spectra).

To gain further insight into the formation of the SEI on uncoated and coated MnO surfaces, "stripes" of ALD Al_2O_3 were patterned on the MnO surface. A series of samples with Al_2O_3 stripes of varying thickness were examined using in situ SICM to image the SEI growth on these intentionally inhomogeneous surfaces. The resulting in situ topographic SICM images for 3, 9, and 90 Å stripes of ALD Al_2O_3 after one electrochemical cycle at a rate of ~15 mA/g are shown in

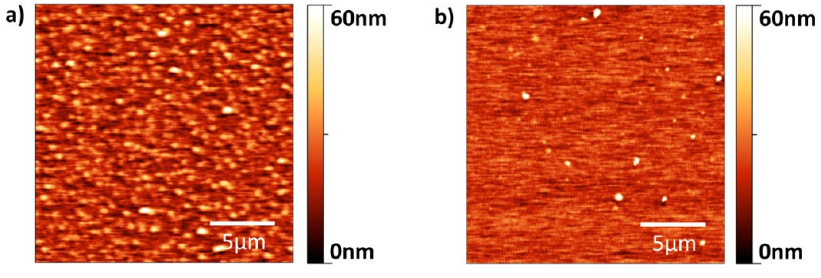

Figure 3. SICM topographical images after lithiation to 0 V for (a) bare MnO and (b) MnO coated with 9 Å of Al_2O_3.

dx.doi.org/10.1021/cm402451h | Chem. Mater. 2014, 26, 935−940

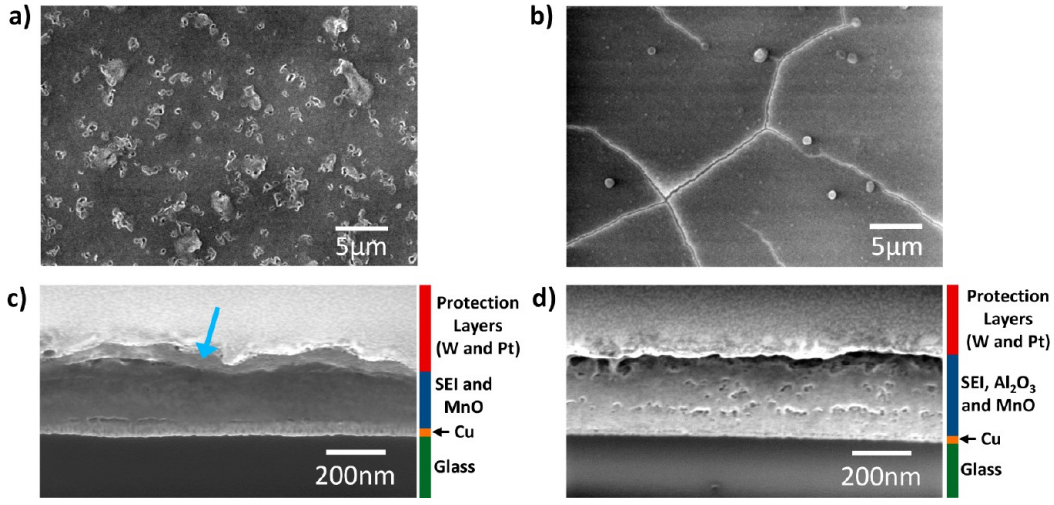

Figure 4. SEM micrographs of (a) the surface and (c) FIB milled cross-sections of bare MnO and (b) the surface and (d) FIB milled cross-sections of 9 Å of ALD Al_2O_3 on MnO after 100 electrochemical charging cycles.

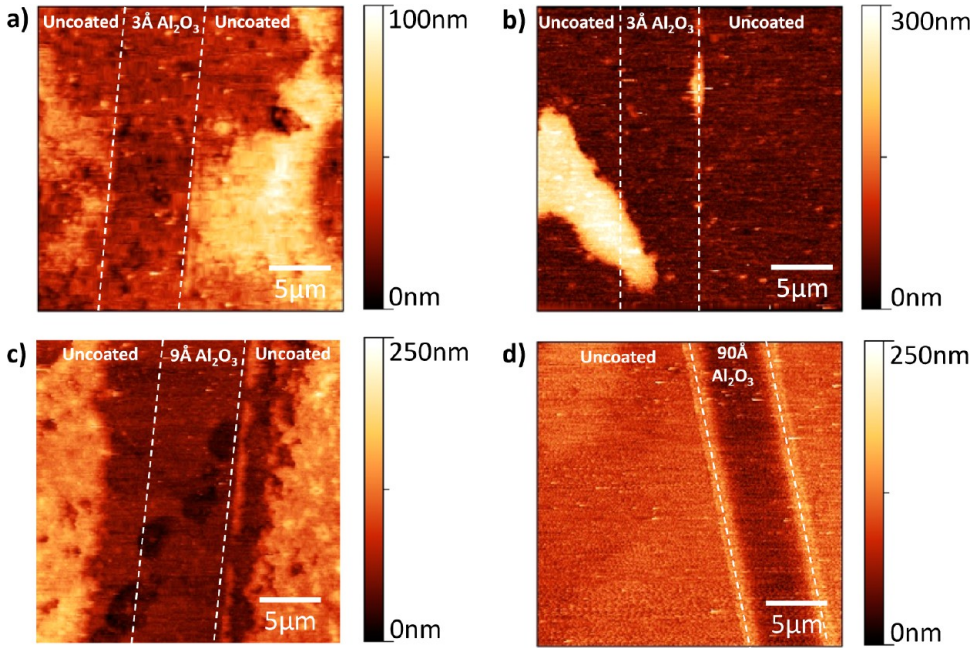

Figure 5. SICM topography images of samples that have undergone one electrochemical cycle with lithographically defined Al_2O_3 stripes on the surface of MnO. (a, b) Two different regions of a sample with stripes of 3 Å thick ALD Al_2O_3 on the surface of MnO. (c) 9 Å thick and (d) 90 Å thick stripes of ALD Al_2O_3.

Figure 5. A coating of 3 Å of ALD Al_2O_3 prevented the formation of a thick SEI layer in some of the coated areas as can be seen in Figure 5a. However, Figure 5b also shows an instance where the SEI has grown over the region of an Al_2O_3 stripe. On average, within a 50 μm × 50 μm image, we observe a small region of this type where the SEI has grown on the ALD Al_2O_3 coating. Thus, a 3 Å thick alumina film appears to only provide a partial reduction in the SEI formation possibly due to the presence of voids or other defects in this ultrathin film. In contrast, for the 9 Å thick ALD Al_2O_3 sample, essentially no SEI is detected over the Al_2O_3 stripes (Figure 5c). In addition, we note that in the completely coated and uncoated samples, shown in Figures 3 and 4, a similar reduction in the SEI was observed indicating that this is not an effect of the striped geometry. Finally, for a thick layer of Al_2O_3 (90 Å thick), there is a clear drop in the height of the Al_2O_3 stripe as compared to the background MnO (Figure 5d). This observation is consistent with Li being unable to diffuse through the thick Al_2O_3 film, thereby preventing expansion of the underlying MnO. This image also confirms that lateral diffusion underneath the stripe is insignificant on the micrometer scale. Unlike the continuous depression observed in Figure 5d for the 90 Å Al_2O_3 stripe, the 3 and 9 Å stripes in images a and c in Figure 4 appear to be SEI-free and similar in height to the surrounding substrate. This finding suggests that for the thinner stripes, approximately the same amount of lithium enters the substrate through the stripes as through the surrounding uncoated MnO. Overall, in situ SICM imaging confirms that ultrathin Al_2O_3 films can inhibit SEI formation, and at 9 Å thickness the SEI formation is practically eliminated.

Following the in situ SICM measurements, an ex situ SEM study was performed on the 9 Å thick patterned sample. In the

dx.doi.org/10.1021/cm402451h | *Chem. Mater.* 2014, 26, 935−940

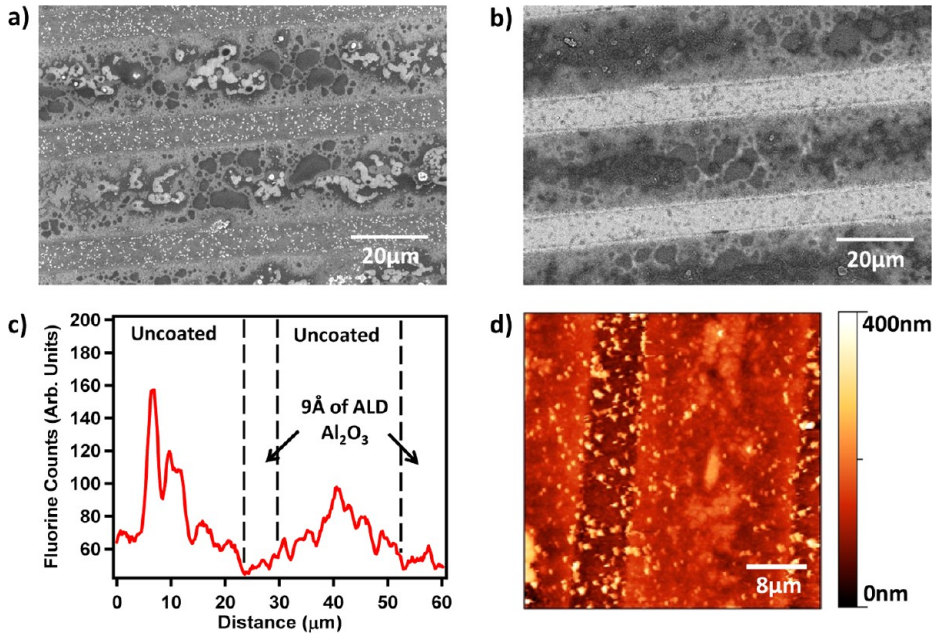

Figure 6. Ex situ characterization of the 9 Å thick stripes of ALD Al_2O_3 on MnO shown in Figure 4c. (a) Secondary electron and (b) backscattered electron SEM micrographs. (c) Fluorine signal from an EDS linescan across 2 stripe periods. (d) AFM topography image.

secondary electron SEM image (Figure 6a), the alumina stripes are observed to be uniform, with the exception of small particles on the surface. These particles appear to be electrolyte residue after the rinsing process, as they were not seen in the in situ SICM images. Backscattered electron images were also obtained to provide elemental contrast (Figure 6b). In particular, the SEI layer is composed of light elements such as Li, C, O, and F and thus should produce relatively few backscattered electrons compared to the heavier Mn in the MnO film. The net result is that a thinner SEI will allow more of the backscattered electrons from the underlying Mn to be detected, resulting in a brighter image. Consequently, the brighter contrast from the stripes compared to the uncoated MnO in Figure 6b suggests a thinner SEI over the Al_2O_3 stripes. To support this finding, an energy-dispersive X-ray spectroscopy (EDS) line scan was obtained across the striped region. Figure 6c shows the resulting F signal as a function of distance across two periods of the Al_2O_3 stripes. In the uncoated region, a higher F signal can be seen as compared to the Al_2O_3 coated stripe, which is consistent with a thicker SEI on the uncoated region.

Finally, ex situ AFM topographic images were gathered on these samples. Although the ex situ AFM image (Figure 6d) is similar to that obtained using in situ SICM (Figure 5c), a major difference is the presence of a large number of particles on and in the vicinity of the Al_2O_3 stripe in the ex situ AFM image that can likely be attributed to electrolyte residue. Furthermore, the Al_2O_3 stripe in the ex situ AFM image appears as an approximately 50 nm depression whereas it was nearly even with the background MnO in the in situ SICM image. This comparison illustrates the unique ability of in situ SICM to minimize contamination and thus investigate battery electrode surfaces without the ambiguities that are present with ex situ characterization methods (e.g., ex situ measurements may mistake electrolyte residue for the SEI).

CONCLUSION

In conclusion, we have performed a nanoscale investigation of SEI formation on ALD Al_2O_3 coated MnO using a combination of in situ and ex situ techniques. In particular, we find that the uncoated MnO surface forms a relatively thick and rough SEI during electrochemical cycling. This SEI can be inhibited with a 3 Å coating of ALD Al_2O_3 and practically eliminated using a 9 Å coating. These thin coatings also survive the rigors of electrochemical cycling for at least 100 cycles and thus continue to prevent SEI formation. These coatings reduce the rate performance of the battery electrode, but this effect can be mitigated by using a high-surface-area electrode. By comparing in situ and ex situ techniques, we have also shown that both methods can provide meaningful information on the SEI, but in situ methods minimize potential artifacts that can occur in ex situ studies. Overall, this study provides unambiguous evidence for the effectiveness of ALD coatings in preventing SEI formation on MnO and presents methodologies for further studies of this effect on other battery electrode materials.

ASSOCIATED CONTENT

Supporting Information

Charge−discharge voltage curves, cyclic voltammetry, X-ray photoelectron spectroscopy spectra of coated and uncoated MnO, and atomic force microscopy of ALD Al_2O_3 stripes of different thicknesses. This material is available free of charge via the Internet at http://pubs.acs.org.

Supporting Information

Additional figures and information (PDF). This material is available free of charge via the Internet at http://pubs.acs.org.

AUTHOR INFORMATION

Corresponding Author

*E-mail: m-hersam@northwestern.edu.

Notes

The authors declare no competing financial interest.

dx.doi.org/10.1021/cm402451h | *Chem. Mater.* 2014, 26, 935−940

■ ACKNOWLEDGMENTS

This research was supported as part of the Center for Electrical Energy Storage, an Energy Frontier Research Center funded by the U.S. Department of Energy, Office of Science, Office of Basic Energy Sciences (Award DE-AC02-06CH11357). M.L.G. acknowledges a National Science Foundation Graduate Research Fellowship. Battery testing instrumentation was funded by the Initiative for Sustainability and Energy at Northwestern (ISEN). This research made use of the NUANCE Center at Northwestern University, which is supported by the NSF-MRSEC (NSF DMR-1121262), Keck Foundation, and the State of Illinois.

■ REFERENCES

(1) Peled, E. *J. Electrochem. Soc.* **1979**, *126* (12), 2047−2051.
(2) Peled, E.; Tow, D. B.; Merson, A.; Gladkich, A.; Burstein, L.; Golodnitsky, D. *J. Power Sources* **2001**, *97*−*8*, 52−57.
(3) Lu, M.; Cheng, H.; Yang, Y. *Electrochim. Acta* **2008**, *53* (9), 3539−3546.
(4) Chattopadhyay, S.; Lipson, A. L.; Karmel, H. J.; Emery, J. D.; Fister, T. T.; Fenter, P. A.; Hersam, M. C.; Bedzyk, M. J. *Chem. Mater.* **2012**, *24* (15), 3038−3043.
(5) Tavassol, H.; Buthker, J. W.; Ferguson, G. A.; Curtiss, L. A.; Gewirth, A. A. *J. Electrochem. Soc.* **2012**, *159* (6), A730−A738.
(6) Abraham, D. P.; Poppen, S. D.; Jansen, A. N.; Liu, J.; Dees, D. W. *Electrochim. Acta* **2004**, *49* (26), 4763−4775.
(7) Aurbach, D.; Markovsky, B.; Salitra, G.; Markevich, E.; Talyossef, Y.; Koltypin, M.; Nazar, L.; Ellis, B.; Kovacheva, D. *J. Power Sources* **2007**, *165* (2), 491−499.
(8) Vetter, J.; Novak, P.; Wagner, M. R.; Veit, C.; Moller, K. C.; Besenhard, J. O.; Winter, M.; Wohlfahrt-Mehrens, M.; Vogler, C.; Hammouche, A. *J. Power Sources* **2005**, *147* (1−2), 269−281.
(9) Wilcox, J. D.; Doeff, M. M.; Marcinek, M.; Kostecki, R. *J. Electrochem. Soc.* **2007**, *154* (5), A389−A395.
(10) Kim, Y. J.; Cho, J. P.; Kim, T. J.; Park, B. *J. Electrochem. Soc.* **2003**, *150* (12), A1723−A1725.
(11) Fey, G. T. K.; Hsiao, C. L.; Muralidharan, P. *J. Power Sources* **2009**, *189* (1), 837−840.
(12) Fu, L. J.; Liu, H.; Li, C.; Wu, Y. P.; Rahm, E.; Holze, R.; Wu, H. Q. *Solid State Sci.* **2006**, *8* (2), 113−128.
(13) Sun, Y. K.; Myung, S. T.; Kim, M. H.; Prakash, J.; Amine, K. *J. Am. Chem. Soc.* **2005**, *127* (38), 13411−13418.
(14) Meng, X.; Yang, X. Q.; Sun, X. *Adv. Mater.* **2012**, *24* (27), 3589−3615.
(15) Ahonen, M.; Pessa, M.; Suntola, T. *Thin Solid Films* **1980**, *65* (3), 301−307.
(16) Scott, I. D.; Jung, Y. S.; Cavanagh, A. S.; An, Y.; Dillon, A. C.; George, S. M.; Lee, S. H. *Nano Lett.* **2011**, *11* (2), 414−418.
(17) Ghosal, S.; Baumann, T. F.; King, J. S.; Kucheyev, S. O.; Wang, Y.; Worsley, M. A.; Biener, J.; Bent, S. F.; Hamza, A. V. *Chem. Mater.* **2009**, *21* (9), 1989−1992.
(18) Jung, Y. S.; Cavanagh, A. S.; Riley, L. A.; Kang, S. H.; Dillon, A. C.; Groner, M. D.; George, S. M.; Lee, S. H. *Adv. Mater.* **2010**, *22* (19), 2172−2176.
(19) Jung, Y. S.; Cavanagh, A. S.; Dillon, A. C.; Groner, M. D.; George, S. M.; Lee, S. H. *J. Electrochem. Soc.* **2010**, *157* (1), A75−A81.
(20) Lahiri, I.; Oh, S. M.; Hwang, J. Y.; Kang, C.; Choi, M.; Jeon, H.; Banerjee, R.; Sun, Y. . K.; Choi, W. *J. Mater. Chem.* **2011**, *21* (35), 13621−13626.
(21) Riley, L. A.; Cavanagh, A. S.; George, S. M.; Jung, Y. S.; Yan, Y.; Lee, S. H.; Dillon, A. C. *ChemPhysChem* **2010**, *11* (10), 2124−2130.
(22) Riley, L. A.; Cavanagh, A. S.; George, S. M.; Lee, S. H.; Dillon, A. C. *Electrochem. Solid State Lett.* **2011**, *14* (3), A29−A31.
(23) Kang, E.; Jung, Y. S.; Cavanagh, A. S.; Kim, G. . H.; George, S. M.; Dillon, A. C.; Kim, J. K.; Lee, J. *Adv. Funct. Mater.* **2011**, *21* (13), 2430−2438.
(24) Ahn, D.; Xiao, X. *Electrochem. Commun.* **2011**, *13* (8), 796−799.
(25) Xiao, X.; Lu, P.; Ahn, D. *Adv. Mater.* **2011**, *23* (34), 3911−3915.
(26) He, Y.; Yu, X.; Wang, Y.; Li, H.; Huang, X. *Adv. Mater.* **2011**, *23* (42), 4938−4941.
(27) Lotfabad, E. M.; Kalisvaart, P.; Cui, K.; Kohandehghan, A.; Kupsta, M.; Olsen, B.; Mitlin, D. *Phys. Chem. Chem. Phys.* **2013**, *15* (32), 13646−13657.
(28) Jung, S. C.; Han, Y. *J. Phys. Chem. Lett.* **2013**, *4* (16), 2681−2685.
(29) Hao, S. Q.; Wolverton, C. *J. Phys. Chem. C* **2013**, *117* (16), 8009−8013.
(30) Leung, K.; Qi, Y.; Zavadil, K. R.; Jung, Y. S.; Dillon, A. C.; Cavanagh, A. S.; Lee, S. H.; George, S. M. *J. Am. Chem. Soc.* **2011**, *133* (37), 14741−14754.
(31) Jeong, S. K.; Inaba, M.; Abe, T.; Ogumi, Z. *J. Electrochem. Soc.* **2001**, *148* (9), A989−A993.
(32) Beaulieu, L. Y.; Cumyn, V. K.; Eberman, K. W.; Krause, L. J.; Dahn, J. R. *Rev. Sci. Instrum.* **2001**, *72* (8), 3313−3319.
(33) Beaulieu, L. Y.; Beattie, S. D.; Hatchard, T. D.; Dahn, J. R. *J. Electrochem. Soc.* **2003**, *150* (4), A419−A424.
(34) Cohen, Y. S.; Aurbach, D. *Electrochem. Commun.* **2004**, *6* (6), 536−542.
(35) Campana, F. P.; Kotz, R.; Vetter, J.; Novak, P.; Siegenthaler, H. *Electrochem. Commun.* **2005**, *7* (1), 107−112.
(36) Clemencon, A.; Appapillai, A. T.; Kumar, S.; Shao-Horn, Y. *Electrochim. Acta* **2007**, *52* (13), 4572−4580.
(37) Lucas, I. T.; Pollak, E.; Kostecki, R. *Electrochem. Commun.* **2009**, *11* (11), 2157−2160.
(38) Balke, N.; Jesse, S.; Morozovska, A. N.; Eliseev, E.; Chung, D. W.; Kim, Y.; Adamczyk, L.; Garcia, R. E.; Dudney, N.; Kalinin, S. V. *Nat. Nanotechnol.* **2010**, *5* (10), 749−754.
(39) Balke, N.; Jesse, S.; Kim, Y.; Adamczyk, L.; Ivanov, I. N.; Dudney, N. J.; Kalinin, S. V. *ACS Nano* **2010**, *4* (12), 7349−7357.
(40) Xu, F.; Beak, B.; Jung, C. *J. Solid State Electrochem.* **2011**, 1−7.
(41) Lipson, A. L.; Ginder, R. S.; Hersam, M. C. *Adv. Mater.* **2011**, *23* (47), 5613−5617.
(42) Pickrahn, K. L.; Park, S. W.; Gorlin, Y.; Lee, H. B. R.; Jaramillo, T. F.; Bent, S. F. *Adv. Energy Mater.* **2012**, *2* (10), 1269−1277.
(43) Burton, B. B.; Fabreguette, F. H.; George, S. M. *Thin Solid Films* **2009**, *517* (19), 5658−5665.
(44) Lu, H. L.; Scarel, G.; Li, X. L.; Fanciulli, M. *J. Cryst. Growth* **2008**, *310* (24), 5464−5468.
(45) Yu, X. Q.; He, Y.; Sun, J. P.; Tang, K.; Li, H.; Chen, L. Q.; Huang, X. J. *Electrochem. Commun.* **2009**, *11* (4), 791−794.
(46) Zhong, K.; Zhang, B.; Luo, S.; Wen, W.; Li, H.; Huang, X.; Chen, L. *J. Power Sources* **2011**, *196* (16), 6802−6808.
(47) Zhong, K.; Xia, X.; Zhang, B.; Li, H.; Wang, Z.; Chen, L. *J. Power Sources* **2010**, *195* (10), 3300−3308.
(48) Zhang, J.; Wang, R.; Yang, X.; Lu, W.; Wu, X.; Wang, X.; Li, H.; Chen, L. *Nano Lett.* **2012**, *12* (4), 2153−2157.
(49) Zhang, Y.; Zhang, X. G.; Zhang, H. L.; Zhao, Z. G.; Li, F.; Liu, C.; Cheng, H. M. *Electrochim. Acta* **2006**, *51* (23), 4994−5000.
(50) Reidies, A. H., *Manganese Compounds*. Wiley-VCH Verlag GmbH & Co. KGaA: 2000.
(51) Yu, X. H.; Bates, J. B.; Jellison, G. E.; Hart, F. X. *J. Electrochem. Soc.* **1997**, *144* (2), 524−532.
(52) Patey, T. J.; Buchel, R.; Nakayama, M.; Novak, P. *Phys. Chem. Chem. Phys.* **2009**, *11* (19), 3756−3761.